Mon. Not. R. Astron. Soc. **000**, 1–?? (2009) Printed 18 February 2010 (MN LATEX style file v2.2)

The evolution of the density of galaxy clusters and groups: denser environments at higher redshifts.

Bianca M. Poggianti[1⋆], Gabriella De Lucia[2], Jesus Varela[1], Alfonso Aragon-Salamanca[3], Rose Finn[4], Vandana Desai[5], Anja von der Linden[6], Simon D.M. White[7].

[1] *INAF-Astronomical Observatory of Padova, Italy*
[2] *INAF-Astronomical Observatory of Trieste, Italy*
[3] *School of Physics and Astronomy, University of Nottingham, United Kingdom*
[4] *Department of Physics, Siena College, Loudonville, USA*
[5] *Spitzer Science Center, California Institute of Technology, USA*
[6] *Kavli Institute for Particle Astrophysics and Cosmology, Stanford University, USA*
[7] *Max-Planck-Institut fur Astrophysik, Garching, Germany*

Accepted .... Received .....; in original form .....

ABSTRACT

We show that, observationally, the projected local density distribution in high-z clusters is shifted towards higher values compared to clusters at lower redshift. To search for the origin of this evolution, we analyze a sample of haloes selected from the Millennium Simulation and populated using semi-analytic models, investigating the relation between observed projected density and physical 3D density, using densities computed from the 10 and 3 closest neighbours. Both observationally and in the simulations, we study the relation between number of cluster members and cluster mass, and number of members per unit of cluster mass. We find that the observed evolution of projected densities reflects a shift to higher values of the physical 3D density distribution. In turn, this must be related with the globally higher number of galaxies per unit of cluster volume N/V in the past. We show that the evolution of N/V is due to a combination of two effects: a) distant clusters were denser in dark matter (DM) simply because the DM density within R_{200} ($\sim$ the cluster virial radius) is defined to be a fixed multiple of the critical density of the Universe, and b) the number of galaxies per unit of cluster DM mass is remarkably constant both with redshift and cluster mass if counting galaxies brighter than a passively evolving magnitude limit. Our results highlight that distant clusters were much denser environments than today's clusters, both in galaxy number and mass, and that the density conditions felt by galaxies in virialized systems do not depend on the system mass.

Key words: galaxies: clusters: general — galaxies: evolution — galaxies: statistics — galaxies: interactions

1 INTRODUCTION

Ever since the work by Dressler et al. (1980) presenting the first morphology-density relation in local galaxy clusters, the projected number density of galaxies (the number of galaxies per unit area or volume) has been a primary tool for investigating the relation between galaxy properties and their environment. Thirty years on, this tool has been applied to galaxies in clusters, groups and the general field, from the local to the high-z Universe, to study the systematic variations of galaxy morphologies, colors, current star formation activity, stellar masses and other galaxy properties with environment (Postman & Geller 1984, Dressler et al. 1997, Hashimoto et al. 1998, Lewis et al. 2002, Gomez et al. 2003, Blanton et al. 2003, Kauffmann et al. 2004, Balogh et al. 2004, Hogg et al. 2004, Postman et al. 2005, Baldry et al. 2006, Cucciati et al. 2006, Cooper et al. 2007, Elbaz et al. 2007, Cooper et al. 2008, Tasca et al. 2009, Bolzonella et al. 2009, to name a few).

More and more sophisticated methods to characterize

⋆ E-mail: bianca.poggianti@oapd.inaf.it

the "local" galaxy density have been scrutinized, and by now a variety of density estimators have been employed in the literature, including the stellar mass density (Wolf et al. 2009), the dark matter density field (Gray et al. 2004), galaxy counts within a fixed metric projected radius and a fixed recession velocity difference (Blanton et al. 2003, Hogg et al. 2004, Kauffmann et al. 2004) and the projected nth-nearest neighbour distance, with the optimal n varying with environment and survey characteristics, sometimes expressed as an overdensity with respect to the median density in the survey (eg. see Cooper et al. 2005 and Kovac et al. 2009 for thorough discussions of different methods). Widely different methods explore different "environmental" conditions and can probe very different physical scales, in some cases over several Mpc, which are far from being a measure of the "local" environment as in the traditional, close neighbour studies in clusters.

Nevertheless, all studies employing the galaxy density share the goal of uncovering the environmental dependence of galaxy properties, and have successfully proved it to be strong. In contrast, little attention has so far been devoted to *how and why density conditions change with redshift*. Observationally, density distributions in clusters at different redshifts have never been compared. In the field, an overdensity is usually measured, factoring out the evolution of the mean density of the Universe, and the evolution of the distribution of environmental conditions beyond that has never been investigated. Theoretical efforts have so far focused on uncovering the physical origin of the observed relations between galaxy properties and density, or have been compared with observations to test the model consistency, or to study the relation between density and halo mass (e.g. Kauffmann et al. 2004, Berlind et al. 2005, Baldry et al. 2006, Elbaz et al. 2008, Gonzalez & Padilla 2009).

A knowledge of the density distribution of galaxies as a function of redshift, and as a function of system mass in virialized systems, would be very useful to assess the changes of local environment experienced by galaxies, but it is currently lacking. In this paper, we analyze the evolution of galaxy densities in clusters, starting from the observed density distribution in distant and nearby clusters. We employ the most traditional of all density estimators, the 10 (or 3) closest neighbours density, as in the original Dressler 1980 work and in most subsequent cluster studies. We compare observations with Millennium Simulation results in order to explain the observed change of the cluster density distribution with redshift, and to relate the evolution in galaxy number density with that of the matter density.

All cluster velocity dispersions σ are given in the rest frame. We assume a ΛCDM cosmology with (H_0, Ω_0, Ω_λ) = (73 $\mathrm{km\,s^{-1}\,Mpc^{-1}}$, 0.25, 0.75).

2 OBSERVATIONS

In this paper we exploit two samples of galaxy clusters: the ESO Distant Cluster Survey (hereafter, EDisCS) at high-z, and a low-z sample from the SDSS. We use the projected local galaxy densities and the total number of members in these clusters as key observables for our study.

The ESO Distant Cluster Survey (hereafter, EDisCS) is a photometric and spectroscopic survey of galaxies in 20 fields containing galaxy clusters at $z = 0.4 - 1$. An overview of the goals and strategy of this survey is given in White et al. (2005) who present the sample selection and the optical ground–based photometry. For all 20 fields EDisCS has obtained deep optical photometry with FORS2/VLT, near-IR photometry with SOFI/NTT, multislit spectroscopy with FORS2/VLT, and MPG/ESO 2.2/WFI wide field imaging in VRI. ACS/HST mosaic imaging in $F814W$ of 10 of the highest redshift clusters has also been acquired (Desai et al. 2007), and a number of multiwavelength follow-up studies have been conducted (see Poggianti et al. 2009 for an overview).

Spectra of > 100 galaxies per cluster field were obtained for 18 out of the 20 cluster fields. The spectroscopic selection, observations, and catalogs are presented in Halliday et al. (2004) and Milvang-Jensen et al. (2008), together with the cluster velocity dispersions. Spectroscopic completeness functions and [OII] line properties as a function of cluster mass are discussed in Poggianti et al. (2006). In this paper we use the projected local galaxy densities computed by Poggianti et al. (2008), who present the star formation-density and morphology-density relations. Our sample consists of 18 clusters and groups at $z = 0.4 - 0.8$ covering a wide range of velocity dispersions ($\sim 200 - 1100\,\mathrm{km\,s^{-1}}$), as listed in Table 1.

At low-z, we use a compilation of 23 clusters and groups at $0.04 < z < 0.1$ drawn from the SDSS, spanning a similar range of velocity dispersions to EDisCS. The sample selection, completeness and data used are fully described in Poggianti et al. (2006). Projected local densities were computed by Poggianti et al. (2008), in a similar way as it was done for EDisCS (see §4).

3 SIMULATION

We make use of the Millennium Simulation (hereafter MS; Springel et al. 2005). The MS follows $N = 2160^3$ particles of mass $8.6 \times 10^8\,h^{-1}\mathrm{M}_\odot$ within a comoving box of size $500\,h^{-1}$Mpc on a side and with a spatial resolution of $5\,h^{-1}$kpc. We extracted 90 haloes at $z = 0.6$ and 90 at $z = 0$ within the simulation box, uniformly distributed in log(mass) between $5 \times 10^{12}\,\mathrm{M}_\odot$ and $5 \times 10^{15}\,\mathrm{M}_\odot$. These are M_{200} masses (hereafter "halo masses"), computed from the simulations as follows. We define R_{200}^{MS} of a FOF-halo as the radius of a sphere which is centered on the most bound particle of the group and has an overdensity of 200 with respect to the critical density of the Universe af the redshift considered. The enclosed mass is defined as M_{200}. For 10-neighbours density measurements, only haloes with more than 10 galaxies brighter than $M_V = -20$ were considered (65 haloes at $z = 0.6$ and 62 at $z = 0$). Dark matter haloes were populated using the semi-analytic model presented in De Lucia & Blaizot (2007), which are publicly available (see also Croton et al. 2006). When deriving quantities to be compared with observations (see next section), in order to take into account projection effects of galaxies close, but not belonging, to the halo, for each halo we considered a box 6Mpc on a side, centred on the most bound particle.

For each halo, we considered all galaxies within 2 R_{200} radii from the central galaxy to compute the projected velocity dispersion along the x, y, and z axes using the same

Table 1. List of clusters.

Cluster	Cluster	z	$\sigma \pm\delta_\sigma$ $\mathrm{km\,s^{-1}}$
Cl 1232.5-1250	Cl 1232	0.5414	$1080\ ^{+119}_{-89}$
Cl 1216.8-1201	Cl 1216	0.7943	$1018\ ^{+73}_{-77}$
Cl 1138.2-1133	Cl 1138	0.4796	$732\ ^{+72}_{-76}$
Cl 1411.1-1148	Cl 1411	0.5195	$710\ ^{+125}_{-133}$
Cl 1301.7-1139	Cl 1301	0.4828	$687\ ^{+81}_{-86}$
Cl 1354.2-1230	Cl 1354	0.7620	$648\ ^{+105}_{-110}$
Cl 1353.0-1137	Cl 1353	0.5882	$666\ ^{+136}_{-139}$
Cl 1054.4-1146	Cl 1054-11	0.6972	$589\ ^{+78}_{-70}$
Cl 1227.9-1138	Cl 1227	0.6357	$574\ ^{+72}_{-75}$
Cl 1202.7-1224	Cl 1202	0.4240	$518\ ^{+92}_{-104}$
Cl 1059.2-1253	Cl 1059	0.4564	$510\ ^{+52}_{-56}$
Cl 1054.7-1245	Cl 1054-12	0.7498	$504\ ^{+113}_{-65}$
Cl 1018.8-1211	Cl 1018	0.4734	$486\ ^{+59}_{-63}$
Cl 1040.7-1155	Cl 1040	0.7043	$418\ ^{+55}_{-46}$
Cl 1037.9-1243⋆	Cl 1037	0.5783	$319\ ^{+53}_{-52}$
Cl 1103.7-1245⋆	Cl 1103	0.7031	$252\ ^{+65}_{-85}$
Cl 1420.3-1236	Cl 1420	0.4962	$218\ ^{+43}_{-50}$
Cl 1119.3-1129	Cl 1119	0.5500	$166\ ^{+27}_{-29}$

Col. (1): Cluster name. Col. (2): Short cluster name. Col. (3) Cluster redshift. Col. (4) Cluster velocity dispersion. Redshifts and velocity dispersions are taken from Halliday et al. (2004) and Milvang-Jensen et al. (2008). Clusters with an asterisk do not have local density measurements, and only their numbers of members are used in this paper.

bi-weight estimator that was used for the EDisCS clusters, and used the mean of these projected velocity dispersions as the velocity dispersion of the system.

4 METHODS – OBSERVED AND SIMULATED MEASUREMENTS

In this section we describe the basic ingredients of our study, and the nomenclature adopted throughout the paper.

For simplicity, in the following we will refer to all galaxy systems of any σ and mass as "clusters", because the distinction between clusters and groups is irrelevant in this paper.

Our analysis is performed within R_{200}, defined as the radius delimiting a sphere with interior mean density 200 times the critical density. R_{200} is often assumed to be approximately equal to the cluster virial radius, since the radius corresponding to a mean interior overdensity of ~ 200 has been shown by N-body simulations to "accurately demarcate the virialized region of the DM halo, which is in approximate dynamical equilibrium, from the exterior, where material is still falling in" (Cole & Lacey 1996). Since most observational studies use R_{200} to compare galaxy properties in clusters at different redshifts, or in clusters and groups of different masses, we use R_{200} to investigate how the density felt by those galaxies that are usually compared observationally changes with redshift and halo mass.

Assuming the virial theorem is valid, from the evolution of the critical density with redshift, R_{200} can be estimated from the observed line-of-sight velocity dispersion as (Finn et al. 2005):

$$R_{200} = 1.73\,\frac{\sigma}{1000\,\mathrm{km\,s^{-1}}}\,\frac{1}{\sqrt{\Omega_\Lambda+\Omega_0(1+z)^3}}\,h_{100}^{-1}\,\mathrm{Mpc} \quad (1)$$

Similarly, from the virial theorem, the cluster mass can be estimated from the velocity dispersion as $M = 1.2\times10^{15}(\frac{\sigma}{1000\,\mathrm{km\,s^{-1}}})^3\times\frac{1}{\sqrt{\Omega_\Lambda+\Omega_0(1+z)^3}}\,h_{100}^{-1}\,M_\odot$ (Finn et al. 2005). In this paper, observed cluster masses are therefore virialized total masses based on observed velocity dispersions derived from spectroscopy. For EDisCS, the latter are in rather good agreement with the velocity dispersions obtained from the weak lensing analysis of Clowe et al. (2006), as shown in Milvang-Jensen et al. (2008).

In the following, we refer to an output value of the simulations either as a "simulated" or a "sim-observed" quantity:

– a *sim-observed* quantity (number of galaxies, velocity dispersion, projected local density etc.) is computed from the simulation with the same method that would be used *observationally*. For example, the sim-observed number of members within R_{200} is the number *in projection* on the XY plane within R_{200} (derived from the velocity dispersion using eqn.(1)) and with a velocity along the Z axis within 3σ from the cluster velocity. No attempt is made to reproduce the cluster selection strategy adopted by EDisCS, nor the geometrical constraints in constructing the masks etc.

– a *simulated* quantity gives the "true" value provided by the simulation. In the example above, this would be the actual number of galaxies inside the sphere defined by the halo R_{200}^{MS} radius.

The difference between simulated and sim-observed quantities is fundamental, as we will show in the paper. Obviously, only sim-observed quantities can be directly compared with observations, but simulated quantities are very useful to address projection issues and other possible observational biases.

4.1 Local densities

All densities in this paper are computed using *proper* (not comoving) quantities, i.e. proper areas and volumes, in Mpc^2 and Mpc^3. This is motivated by the fact that, in order to study the dependence of galaxy properties on the density of the local environment, what matters are gravitational and vicinity effects, and therefore proper distances between galaxies.

Projected local galaxy densities were computed from the observations as described in detail in Poggianti et al. (2008) using the circular area that in projection on the sky encloses the 10 closest galaxies brighter than an absolute V magnitude $M_V = -20$.

From the simulation, we compute both the sim-observed projected 2D local density and the physical 3D density.

Sim-observed projected local densities are computed for each galaxy "member" (sim-observed member) of a simulated cluster as for observations: we consider as members all galaxies brighter than a limit M_V (either -20 or -19.4, see below) within a projected radius R_{200} from the "BCG" (the central galaxy of the halo) and within 3σ in velocity from the mean cluster velocity. The projected local density Σ (gal/Mpc^2) is calculated from the ratio n/Area where Area is the circular area encompassing the n projected clos-

est neighbours brighter than M_V in the XY ("sky") plane, with $n = 10$ unless otherwise stated.

The "physical" local density ρ (gal/Mpc^3) is meant to measure the 3D number density of a region around each galaxy. It is computed as the ratio n/Volume, where the Volume is the spherical volume encompassing the n closest neighbours in 3D brighter than M_V, with $n = 10$ unless otherwise stated. The 10 closest neighbours to each galaxy are those with the 10 smallest values of distance $d = sqrt((\delta x)^2 + (\delta y)^2 + (\delta z)^2)$ from the galaxy, where $(\delta x, \delta y, \delta z)$ are the distances along each axis in the simulation.

When computing the densities from the simulation, all neighbours above the magnitude cut were considered, also if outside R_{200}^{MS}, to avoid edge effects at the radius R_{200}^{MS}, similarly to what was done observationally.

5 RESULTS - THE EVOLUTION OF THE LOCAL DENSITY DISTRIBUTION

Observationally, the projected local density distribution in low-z clusters is shifted towards lower values compared to clusters of similar masses at higher redshift. This is shown in Fig. 1, and was mentioned in Poggianti et al. (2008). This could also have been inferred if someone had compared previous low-z (Dressler 1980, Lewis et al. 2002) and high-z (Dressler et al. 1997, Postman et al. 2005) cluster observations.

To our knowledge, the evolution of the observed density distribution, its origin and consequences have not been discussed in the past. It may be argued that this effect could be due to density measurements at high-z suffering from a higher contamination of interlopers, that can artificially inflate the observed densities, but we will show this is not the case.

In order to understand the significance of the density evolution, we investigate how the observed 2D projected density distribution at different redshifts is related to the physical 3D density distribution in the simulation, and how both are expected to change with redshift in clusters.

Observations and simulations are compared in Fig. 1 for galaxies brighter than $M_V \leqslant -20$. Only haloes with $M > 10^{14}$ M$_\odot$ are used in this comparison, to match the masses of EDisCS and SDSS clusters that dominate the observed density distribution.

The observed projected density distribution (red histograms) shifts by about 0.4dex from $z = 0.6$ to $z = 0$, corresponding to a decrease by a factor 2.5. Sim-observed projected densities evolve by the same amount (black histograms), and they follow rather well the observed projected density distributions both at high- and low-z.

The corresponding 3D physical densities computed from the simulation are shown in the left panel of Fig. 2. The evolution of the physical 3D densities is even stronger than that of the 2D distribution. Physical densities for $M_V = -20$ were on average higher by 0.5 dex, that is a factor ~ 3.2, in distant clusters than today. Therefore, the evolution in projected density is not merely a projection effect with z, but corresponds to physically evolving conditions in 3D galaxy number density.

It is also interesting to note that, when accounting for the average observed shift and rescaling to the same number of galaxies, the 2D and 3D density distributions at $z = 0$ closely match the respective distributions at $z = 0.6$ (see dashed histograms in Fig. 2). After number rescaling, the high-z distribution can be obtained with good approximation from the low-z histogram simply multiplying each density by a factor ~ 3.2 in 3D, and 2.5 in 2D, since the shape of the distribution does not change.

Importantly, we find that both the 2D and the 3D density distributions do not vary strongly with cluster mass, as shown in Fig. 3.[1] The $n = 10$ neighbours physical density distribution are rather similar at all halo masses above $M = 10^{14}$ M$_\odot$ (top panels), covering the same range of densities. The binned distributions shown in Fig. 3 do not overlap with each other for always less than 12% of the galaxies. At lower halo masses, $M = 0.3 - 1 \times 10^{14}$ M$_\odot$, corresponding to the lowest mass groups in EDisCS, using $n = 10$ is inappropriate because the number of luminous members is less than 10 for many systems. Using densities computed for $n = 3$ (bottom panels in Fig. 3), the density distributions remain rather similar to those of more massive clusters. Galaxies in haloes with masses $M = 0.3 - 1 \times 10^{14}$ M$_\odot$ cover the same density range of galaxies in more massive haloes, and the 3D density distributions do not overlap in less than 15% of the galaxies. Remarkably, this means that the distributions of local densities to the 3 closest neighbours are quite similar for galaxies in clusters over two orders of magnitude in mass, suggesting that there is an approximately equal distribution of dense and less dense regions from groups to massive clusters when the "really local" density is considered. The intuitive belief that more massive clusters are denser environments proves to be wrong. Actually, we see that the lowest halo mass bin has the largest 3D high-density tail.

So far we have used a fixed $M_V = -20$ galaxy magnitude limit at both redshifts, but it is physically more meaningful to adopt an M_V limit evolving with redshift, taking into account the fact that a galaxy luminosity evolves as the galaxy stars become older. We consider passive evolution, that is the evolution of an integrated spectrum due to simple aging of old stellar populations, without the addition of any new star. Using van Dokkum & Franx (2001) or, equivalently, Fritz et al. (2007) spectrophometric models for a single episode of star formation occurred at z between 1.5 and 3 for a Salpeter IMF and solar metallicity, the evolution of M_V between $z = 0.6$ and 0 is 0.5-0.7mag.[2] Therefore, we

[1] Although a wider study as a function of the cluster delimiting radius is beyond the scope of this paper, we have verified that the galaxy 3D number density distribution does not vary strongly with cluster mass also when using a smaller radius, R_{500}, the radius whose interior mean density is equal to 500 times the critical density.

[2] As pointed out by Conroy, Gunn & White (2009), the uncertainties in the IMF slope at low stellar masses translate into an uncertainty in the passively evolving luminosity evolution of 0.4mag in K between $z = 1$ and $z = 0$. If we arbitrarily assume the uncertainty to be the same in V and in K, the change in luminosity over our redshift range due to the IMF is still much smaller than that obtained lowering the star formation redshift to e.g. $z = 1$. Thus, the uncertainty in the passively evolving magnitude limit is dominated by the assumption in the formation redshift of most stars. The great majority of cluster galaxies have very old mass-weighted stellar ages (e.g. Fritz et al. 2010, in prep.)

consider an evolving magnitude limit going from $M_V = -20$ at $z = 0.6$ to $M_V = -19.4$ at $z = 0$.

Passive evolution produces a stronger decreasing luminosity evolution than any other star formation history. Therefore, assuming a passively evolving magnitude limit, we are sure to include in the density calculation at $z = 0$ all galaxies that would be included at $z = 0.6$, and possibly some more galaxies that do not make it into the sample at $z = 0.6$. This yields a sort of lower limit on (but is probably close to)[3] the evolution of the density distribution as it would be measured using a fixed galaxy stellar mass limit and if galaxy masses did not evolve significantly.[4] On the contrary, the non-evolving $M_V = -20$ used above excludes from the low-z density calculation all those galaxies that have faded below the limit by $z = 0$ but were included at $z = 0.6$. Therefore, it provides an upper limit for the evolution of the density distribution for a mass-limited galaxy sample with non-evolving galaxy masses.

Unfortunately, the SDSS spectroscopy is not deep enough to reach $M_V = -19.4$ in our SDSS clusters. Adopting a brighter, passively evolving limit at both redshifts would result in too few galaxies in high-z clusters to allow a robust density determination. Hence, we are forced to investigate the passive evolution case only in the simulation, mimicking the way a sufficiently deep observational survey at low-z would be treated to compare with the high-z results. The fact that the observed $M_V = -20$ density distributions are well reproduced in the simulation, as is the number of cluster members shown in the next section, makes us confident that the simulated densities should be reliable also down to 0.5 magnitude fainter.

With a passively evolving galaxy magnitude limit, the shifts of the 2D and 3D density distributions in the simulation are smaller, but still conspicuous (Fig. 4). After number rescaling, the high-z 3D and 2D density distributions match the $z = 0$ distributions if densities decrease by a factor ~ 1.8 (0.25dex) in 3D and 1.6 (0.2dex) in 2D.

The analysis of the simulations presented so far demonstrates that, within R_{200} and computing local densities from the 10 or 3 closest neighbours, a) distant clusters were denser environments than low-z clusters, in the sense that, at $z = 0.6$, cluster galaxies had on average $\sim 2 - 3$ times (> 0.25dex, < 0.5dex) more luminous/massive neighbors than at $z = 0$, and b) the distribution of physical densities is rather similar in haloes over two orders of magnitude in mass.

therefore a high formation redshift range as the one adopted here is appropriate.

[3] It should be close to the evolution of the density distribution in a galaxy stellar mass limited sample because the majority of bright galaxies as those considered here have a negative luminosity evolution very close to passive, having truly passively evolving or declining star formation histories.

[4] Note that the simulation, by its own nature, does not assume conservation of galaxy numbers, nor galaxy masses, since it includes galaxy mergers.

6 THE CAUSE OF THE DENSITY EVOLUTION IN A COSMOLOGICAL FRAMEWORK

In the analysis presented above, densities represent *number densities* of galaxies, that means number of neighbours of an individual galaxy down to a certain magnitude, per unit of projected area or volume. In the following we want to establish

- how the evolution in number density of individual galaxies corresponds to the evolution of the *global average number density* over the whole cluster (total number of members per unit volume N/V). In doing this, we investigate separately the evolution of N within R_{200} and the evolution of the volume V enclosed by R_{200}. The question we wish to address is how the change of the 3D number density with redshift is related to the evolution of N/V, and N and V separately, and how and why these evolve. Note that N/V can be estimated observationally, by estimating a cluster radius from either σ or an alternative mass measurement, and counting the number of members within this radius.
- how the *number* density evolution is related to the mean *matter* density evolution in clusters, that is the evolution of the mean total, or DM, mass per unit volume. In principle, mass density and number density are different measurements of environment, and are expected to influence physical processes in different ways: for example, number density is more relevant for galaxy-galaxy interactions and mergers, while mass density is more relevant for other effects, such as the cluster tidal field. We wish to understand if number densities and mass densities evolve in similar or different ways, to gain a more complete picture of the evolution of environmental conditions.

The number of galaxies per cluster observed in the EDisCS and Sloan datasets within R_{200} is shown as a function of the observed velocity dispersion in Fig. 5. This is compared at each redshift with the sim-observed number of galaxies as a function of sim-observed velocity dispersion. From Fig. 5, it can be seen that the sim-observed numbers agree quite well with the observed numbers at both redshifts, although the sim-observed numbers at $z = 0$ tend to be slightly higher than the observed values by about 0.1dex.

The number of galaxies increases with velocity dispersion at both redshifts (higher velocity dispersion clusters have more members, obviously). For a fixed $M_V \leqslant -20$ limit, the number of members decreases from $z \sim 0.6$ to $z \sim 0$ (the number of galaxies down to a fixed magnitude limit in a cluster of a given σ was higher in the past), as shown by the offset in the right panel between the high-z best-fit line and the $z = 0$ points.

Since clusters with the same observed velocity dispersion but different redshift have different masses (cf. §4), we remove this effect by plotting the number of galaxies versus cluster mass in Fig. 6, see bottom panels. The trends remain similar: both observationally and theoretically, the number of galaxies increases linearly with mass in a log-log plot, and, for a fixed galaxy magnitude limit, it decreases towards lower redshift.

To understand if the number decline at lower redshift is simply due to galaxies dropping off the sample at $z = 0$ because they fade below the fixed magnitude cut, in Fig. 5

and Fig. 6 we also show the sim-observed number of cluster members for a passively evolving magnitude limit $M_V = -19.4$ at $z = 0$ (blue points). As explained in §5, we cannot do the same observationally, because the SDSS spectroscopy is not deep enough. With the passively evolving limit, the numbers at $z = 0$ in the bottom right panel of Fig. 6 are only 0.057dex lower than the best fit $z = 0.6$ correlation shown by the solid line ($LogN = (0.77 \pm 0.03) \times LogM + (1.43 \pm 0.02)$). As we will discuss later in this section, this residual small mismatch is caused by the way masses are derived, and the effect disappears when "true" simulated masses of haloes are considered (top right panel in Fig. 6).

To conclude, both observations and simulations show a mild evolution in the N vs M relation with redshift for a fixed magnitude limit. When passive evolution is taken into account, the number of members in a cluster of a given mass does not evolve between $z \sim 0.6$ and $z = 0$. A similar result was found by Lin et al. (2006), who, based on cluster mass estimates derived from the X-ray temperature and observed number counts, concluded that for passive evolution the $N-M$ relation shows no sign of evolution out to $z = 0.9$.

This result implies that the evolution in the number density distributions for the passive evolution case in cluster samples with the same cluster mass distribution at different redshifts (Fig. 4) is not due to a higher number of members at $z = 0.6$, but must originate mostly from the "expanded size" of local clusters compared to distant ones, that is, to the evolution of the cluster volume.

6.0.1 *A recollection of the evolution of cluster volume and dark matter density*

At this point it is useful to recall some textbook knowledge about how and why the volume and the mean matter density of clusters evolve, and how this evolution simply stems from using R_{200} to define both of them.

Due to the expansion of the universe, a unit volume today corresponds to a volume smaller by a factor $1/(1+z)^3$ at redshift z (Peebles 1993). Therefore, the physical 3D density (number of galaxies per unit volume) of non-evolving objects locked into the Hubble flow changes with redshift as $(1+z)^3$. Galaxies and clusters of galaxies, however, are far from being unevolving objects, with clusters accreting new galaxies and groups. Moreover, collapsed structures such as clusters should have broken off from the Hubble flow, at a time when their density exceeded a fixed multiple of the critical density at that redshift (Peebles 1993, Cole & Lacey 1996).

Since we only include galaxies within the cluster R_{200}, *by definition* the mean *matter* density within this radius is 200 times the critical density at that redshift. The critical density evolves with z as:

$$\varrho_c(z) = \frac{3{H_0}^2}{8\pi G} \times (\Omega_\lambda + \Omega_0(1+z)^3) \qquad (2)$$

where G is the gravitational constant $= 4.29 \times 10^{-9}\,(\mathrm{km/s})^2\,\mathrm{Mpc\,M_\odot}$.

As a consequence, the mean matter density (= mass per unit volume) in clusters of *any mass*, within a radius $R = R_{200}$ goes as:

$$\begin{aligned} \varrho_m(z) &= \frac{M}{V} = \frac{M}{(4/3)\pi R_{200}^3} = 200\varrho_c(z) \\ &= 200 \times \frac{3{H_0}^2}{8\pi G} \times (\Omega_\lambda + \Omega_0(1+z)^3) \\ &= a + b(1+z)^3 \end{aligned} \qquad (3)$$

where $a = 200 \times \frac{3{H_0}^2}{8\pi G} \times \Omega_\lambda = 22.241 \times 10^{12}\,\mathrm{Mpc^{-3}\,M_\odot}$ and $b = 200 \times \frac{3{H_0}^2}{8\pi G} \times \Omega_0 = 7.414 \times 10^{12}\,\mathrm{Mpc^{-3}\,M_\odot}$ in our cosmology.

This means that *the mean matter density in clusters at a given redshift is the same for all clusters*. Moreover, it means that *the mean matter density evolves in the same way for clusters of all masses*, by a factor $\varrho_1/\varrho_2 = (a+b(1+z_1)^3)/(a+b(1+z_2)^3)$ between z_1 and z_2. This has a number of implications, all consequences of using R_{200} as the radius delimiting the cluster, among which:

- The mean matter density within a cluster R_{200} at any redshift can be computed from eqn.(3): the most distant cluster at z_1 has a density $(a + b(1+z_1)^3)/(a + b(1+z_2)^3)$ times higher than a cluster at z_2. In our case, any cluster at $z = 0.6$ (of any mass) has a matter density $52.61 \times 10^{12}\mathrm{M_\odot\,Mpc^{-3}}$, and any cluster at $z = 0$ has $\varrho_m = 29.65 \times 10^{12}\mathrm{M_\odot\,Mpc^{-3}}$, a factor of 1.774 less dense. The larger the redshift difference, the stronger the evolution: between $z = 1.0(1.5)$ and $z = 0$, the matter density evolves by a factor 2.750(4.656).
- Equation (3) implies that two clusters of the same mass $M_1 = M_2$ but different redshifts z_1 and z_2 have different volumes: the most distant cluster at z_1 has a volume $(a + b(1+z_2)^3)/(a + b(1+z_1)^3)$ times smaller than the other (1.774 times smaller at $z = 0.6$ compared to $z = 0$). The ratio of the volumes of two equal mass clusters at different redshifts is therefore invariant with the cluster mass, and only depends on redshift, while, at any given redshift, the volume is linearly proportional to the mass (eqn. 3): a cluster twice as massive has twice as large a volume.[5]

6.1 The constancy of the number of galaxies per unit cluster mass, and the evolution of the number of galaxies per unit volume

The number of cluster members divided by the cluster mass N/M is presented in Fig. 7 as a function of cluster mass. The sim-observed quantities agree well with the EDisCS and SDSS datapoints (top left and right panels). Both observations and simulation show a strong trend of declining N/M with mass, with a shift to lower N/M at lower z when the

[5] One might wonder how mass M and volume V, separately, change in an evolving individual cluster(halo), considering that on average M grows with z by a factor that is larger at larger masses, as shown by numerous theoretical works (eg. Lacey & Cole 1993). Simulations show that the average mass growth between $z = 0.6$ and $z = 0$ is about 1.5 times for 1.1×10^{12} (mass at $z = 0.6$), about 1.9 for 5.6×10^{13}, 2.35 for 3.7×10^{14}, and 3.0 for $\sim 10^{15}$ (the mass growth for finer intervals of cluster masses can be found in Table 4 of Poggianti et al. 2006). The independence of ϱ_m from the cluster mass (eqn. 3) implies that, although the mass growth rate depends on cluster mass, the parallel evolution in cluster volume (radius) compensates the mass dependence.

$M_V = -20$ limit is used. Accounting for passive evolution (blue points in the bottom left panel), the $z = 0$ trend almost overlaps with that at $z = 0.6$, as was already shown in Fig. 6.

The observed and predicted declining N/M trend with mass seems to suggest that more massive clusters have a lower number of galaxies per unit of cluster mass. We will now show that this is just an illusory result due to the way the mass is computed "observationally". In fact, we find there is a discrepancy in the simulations between the halo masses and the mass derived from the sim-observed velocity dispersion (Fig. 8). Masses derived from the sim-observed velocity dispersion underestimate the halo masses by up to an order of magnitude in low-mass groups ($M_{sim-obs} \leqslant 4\times10^{13}\,M_\odot$). They yield halo mass values with good approximation at intermediate masses ($M_{sim-obs} = 4\times10^{13}\,M_\odot - 4\times10^{14}\,M_\odot$), and slightly overestimate the halo masses for massive clusters ($M_{sim-obs} > 4\times10^{14}\,M_\odot$). The correlation is $log(M_{sim-obs}) = (1.325 \pm 0.04) \times M_{simul} - (0.21 \pm 0.02)$, where both masses are in units of $10^{14} M_\odot$. The top panels of Fig. 6 shows that, using halo masses, the correlation between number of galaxies and cluster mass steepens ($LogN = (1.00 \pm 0.04) \times LogM + (1.29 \pm 0.02)$), and passively evolved points at $z = 0$ follow the same exact $N - M$ correlation found at $z = 0.6$ with no offset (top right panel, blue points).

The mass discrepancy corresponds to a discrepancy in both σ and cluster radius: the sim-observed velocity dispersion and sim-observed R_{200} deviate from the velocity dispersion obtained from the halo mass and from the theoretical R_{200}^{MS} radius, underestimating them at low values and overestimating them at high values (middle and right panels of Fig. 8).

The mismatch between halo masses and cluster mass estimators based on velocity dispersion was studied in detail by Biviano et al. (2006), whose results agree very well with ours. Based on cosmological hydrodynamical simulations, they studied clusters with masses above $10^{14}\,M_\odot$ considering several observational effects such as the presence of interlopers and subclusters, sample size, incompleteness and different tracers of gravitational potential (different types of galaxies and DM particles). For masses below $10^{14}\,M_\odot$, where we find the strongest mismatch between the two types of masses, we are not aware of any previous work we can compare with.

The bottom right panel of Fig. 7 presents the number of cluster members per unit cluster mass obtained using the halo mass in the simulation instead of the sim-observed mass derived from the sim-observed velocity dispersion. The decline with cluster mass disappears: the ratio between number of members and cluster mass is constant with mass and, when passive evolution is included, is constant also with redshift. There appear to be, on average, approximately 20 galaxies brighter than a passively evolving $z = 0$ limit $M_V = -19.4$ for each $10^{14}\,M_\odot$ of cluster mass, for any mass, at both redshifts.[6] This constancy is remarkable, also because it applies over a two order magnitude range of cluster mass, and regardless of redshift at least up to $z = 0.6$.

The fact that simulations are able to reproduce the observed $Log(N/M)$ vs $LogM$ trends (upper panels of Fig. 7), and that such trends disappear when adopting the halo mass instead of the sim-observed mass (hence, when simply removing projection effects that bias the observational estimate of the halo mass) supports the validity of the constancy of N/M, regardless of the prescriptions of the semi-analytic model.

This constancy, and the small scatter around the mean value, especially in massive clusters ($Log(N/M(10^{-14}M_\odot)) = (1.29 \pm 0.10)$ for haloes with $M > 10^{14}M_\odot$, and $Log(N/M(10^{-14}M_\odot)) = (1.26 \pm 0.22)$ for $M < 10^{14}M_\odot$), suggests that measuring N should be a powerful method to estimate the cluster mass, free from the systematic mismatch between "true" halo mass and σ-based mass estimate. Recall that N can be observationally estimated as the number of members brighter than our passively evolving limit within R_{200}, if an estimate of R_{200} is available. The constancy of N/M should allow to start from a first guess for N within a fixed metric radius (see also Andreon & Hurn 2009), derive the mass, the corresponding R_{200} and N within this radius, iterating the procedure until convergence at $N/M \sim 20$ is reached. Further investigation, combining simulations and observations, would be valuable to assess the utility of this method, comparing other observed cluster samples, at different redshifts, with simulations as in Fig. 7). This should test the model capability to reproduce the observed N and, most importantly, compare the mass estimate precision with that of other methods, especially those based on other definitions of richness that do not consider the N/M constancy found in this paper (see e.g. Popesso et al. 2005, Gladders et al. 2007, Rozo et al. 2009, Andreon & Hurn 2009).

Since our simulations show that for passive evolution and using halo masses, the average N/M is constant both with z and M (Fig. 7), and given that $V = M/(a+b(1+z)^3)$ (from eqn(3)), the number of galaxies per unit volume goes as:

$$N/V = c \times (a + b(1 + z)^3) \quad (4)$$

where $c = N/M \sim 20\,\mathrm{gal}/10^{14}\mathrm{M}_\odot$.

Therefore, *both the mean matter density* (mass per unit volume, eqn. 3) and the average *global number density* (number of members per unit volume, eqn. 4) depend only on redshift, not on cluster mass, and are higher in more distant clusters by the same factor $(a + b(1 + z_1)^3)/(a + b(1 + z_2)^3)$ with $z_1 > z_2$.

We have seen that between $z = 0.6$ and $z = 0$ this factor is equal to 1.774 (0.25dex) in our cosmology. This is in striking agreement with, and accounts for, the 0.25dex shift of the 3D individual number density distribution shown in Fig. 4, and it must be ultimately responsible for the higher projected number densities observed at higher redshift (Fig. 1).

To summarize, our results show that higher-z clusters are denser than lower-z clusters, both in individual and global number density of galaxies, and in mass. The constancy of the average *mass* density with cluster mass, and its evolution with redshift, is simply a consequence of the evo-

[6] This result is unchanged if we use the "real" simulated instead of the sim-observed number of members, i.e. also the simulated average N/M ratio is constant with mass and redshift.

lution of the critical density and of considering as "cluster" only the region within R_{200} which approximates the sphere of influence of cluster gravity against the Hubble flow.

Not at all obvious was the fact that also the *global number* density should follow the same laws, should be independent of cluster mass and should evolve as the mass density. We have demonstrated that this is true because the number of galaxies per unit of cluster mass N/M is invariant *both with cluster mass and redshift*, when passive evolution is taken into account and when masses are unaffected by observational biases. Far from obvious was also the evolution of the projected and the 3D galaxy number density distributions, whose shape does not change with redshift and whose mean evolves exactly as the global number density.

Interestingly, these conclusions apply to any virialized system regardless of its mass, thus should be applicable from the most massive clusters to the least massive groups. It may appear counterintuitive, but we have just shown that the *average* surrounding number and mass density seen by a galaxy in any virialized region is the same at a given redshift, regardless whether the galaxy belong to a small group, an intermediate mass or a massive cluster. In the previous section, we have also shown that not only the average density, but also the number density *distribution* is approximately the same in the virialized regions of all halo masses explored. As far as densities are concerned, on large and unbiased cluster samples, the mass of the system does not matter, epoch does.

However, it is fundamental to keep in mind that, while the density average and, approximately, distributions are independent of cluster mass, there is a scatter in the predicted N/M (and therefore N/V and 3D distribution) *at any given mass*, a scatter that increases towards lower halo masses, as visible in Fig. 7 and testified by the larger scatter (0.22 versus 0.10) in the $Log(N/M)$ relations given earlier in this section. Cluster-to-cluster density variations at a given mass are therefore not described in this formalism, but should be important for individual clusters expecially below $10^{14}\,M_{\odot}$, and likely will depend on the specific cluster growth history.

7 SUMMARY

1) The observed distribution of projected local densities in high-z clusters is shifted to higher values compared to the low-z distribution, and is reproduced by simulations. Based on the 3D density distributions obtained from the simulations, we find that this is due to high-z clusters being denser, in physical space, than their local counterparts. Galaxies in distant clusters are therefore on average closer to each other than galaxies in local clusters.

2) The shift to higher individual galaxy number densities at higher redshifts is consistent with the globally higher number of galaxies per unit volume on the cluster scale that we obtain from the way the cluster region is defined and from the simulation results. The number of galaxies per unit volume is higher by approximately a factor 1.8 at $z = 0.6$, and a factor 4.7 at $z = 1.5$, compared to $z = 0$.

3) We find that the global number density N/V evolves because of the combination of two effects: the DM mass per unit volume (the mass density) increases at higher redshift, simply because the cluster R_{200} radius is defined to enclose a density that is 200 times the critical density, while simulations show that the average number of galaxies per unit of DM mass N/M is constant both with redshift and cluster mass, being always $\sim 20\,\mathrm{gal}/10^{14}\mathrm{M}_{\odot}$ counting only galaxies brighter than a passively evolving $M_V = -19.4$ at $z = 0$.

The constancy of N/M is found when considering the DM halo mass, but does not persist when using sim-observed masses derived from the velocity dispersion as it is done observationally, because the latter strongly underestimate the system mass at low masses, and slightly overestimate it at high masses. In the case of sim-observed masses derived from velocity dispersions, simulations show a decline of N/M with mass, in agreement with the observed relations both at high- and low-z.

4) From the previous point, it stems that both the mass density and the global number density evolve as the critical density and do not depend on cluster mass, therefore they are the same for clusters of all masses, at a given redshift. Moreover, the distribution of physical number densities obtained from the simulations does not vary strongly with cluster mass. Hence, contrary to the most intuitive belief of more massive systems being denser, mentioned in many observational studies, the most massive and the least massive clusters or groups are on average equally dense, at a given redshift.

It is important to keep in mind that these conclusions apply to *virialized regions* and for the density estimators adopted in this paper, that is for a method using the 10 (and, we have verified, also 3) closest neighbours. These conclusions cannot be blindly applied to other types of density estimates that probe physically different scales, nor can be expected to hold in unvirialized regions of the Universe. For example, the observed shift in 3D densities with redshift cannot simply be assumed to be valid also when density is measured as number counts within a 8 Mpc sphere or a $2\mathrm{Mpc}\times2\mathrm{Mpc}\times500\mathrm{km\,s}^{-1}$ cylinder in a general field survey.

Moreover, we note that in principle these results may depend on the semi-analytic model employed, but this can only be ascertained repeating the analysis with other models.

Our results highlights two main aspects:

a) the strong evolution in the average density conditions experienced by galaxies in clusters. More distant systems are much denser environments, both in number and in DM ($\sim$ total)mass.

b) the impressive homogeneity in the density of clusters regardless of mass, at a given redshift. Not only the DM mass density, but also the average number density of galaxies and, approximately, the distribution of physical number densities are the same in the virialized regions of clusters and groups of any mass, at a given redshift. Cluster-to-cluster variations *at a given mass*, however, may be important for individual systems, especially at masses below $10^{14}M_{\odot}$.

ACKNOWLEDGMENTS

BMP thanks the Alexander von Humboldt Foundation and the Max Planck Instituut fur Extraterrestrische Physik in Garching for a very pleasant and productive staying during which the work presented in this paper was carried out. The Millennium Simulation data bases used in this paper and

the web application providing online access to them were constructed as part of the activities of the German Astrophysical Virtual Observatory. BMP acknowledges financial support from ASI contract I/016/07/0. GDL acknowledges financial support from the European Research Council under the European Community's Seventh Framework Programme (FP7/2007-2013)/ERC grant agreement n. 202781.

REFERENCES

Andreon, S., Hurn, M.A., 2009, MNRAS, submitted
Baldry, I.K., Balogh, M.L., Bower, R.G., Glazebrook, K., Nichol, R.C., Bamford, S.P., budavari, T., 2006, MNRAS, 373, 469
Balogh, M.L., Baldry, I.K., Nichol, R., Miller, C., Bower, R., Glazebrook, K., 2004, ApJ, 615, L101
Berlind, A.A., Blanton, M.R., Hogg, D.W., Weinberg, D.H., Dave', R., Eisenstein, D.J., Katz, N., 2005, ApJ, 629, 625
Biviano, A., Murante, G., Borgani, S., Diaferio, A., Dolag, K., Girardi, M., 2006, A&A, 456, 23
Blanton, M.R., et al., 2003, ApJ, 594, 186
Bolzonella, M., et al., 2009, A&A in press (arXiv: 0907.0013)
Clowe, D., et al., 2006, A&A, 451, 395
Cole, S., Lacey, C., 1996, MNRAS, 281, 716
Conroy, C., Gunn, J.E., White, M., 2009, ApJ, 699, 486
Cooper, M.C., Newman, J.A., Madgwick, D.S., Gerke, B.F., Yan, R., Davis, M., 2005, ApJ, 634, 833
Cooper, M.C., Newman, J.A., Weiner, B.J., et al., 2007, MNRAS, 376, 1445
Cooper, M.C., Newman, J.A., Weiner, B.J., et al., 2008, MNRAS, 383, 1058
Croton, D.J., Springel, V., White, S.D.M., De Lucia, G., Frenk, C.S., Gao, L., Jenkins, A., Kauffmann, G., Navarro, J.F., Yoshida, N., 2006, MNRAS, 365, 11
Cucciati, O., Iovino, A., Marinoni, C., et al., 2006, A&A, 458, 39
De Lucia, G., Blaizot, J., 2007, MNRAS, 375, 2
Desai, V., et al., 2007, ApJ, 660, 1151
Dressler, A. 1980, ApJ, 236, 351
Dressler, A., Oemler, A., Couch, W.J., Smail, I., Ellis, R.S., Barger, A., Butcher, H., Poggianti, B.M., Sharples, R.M., 1997, ApJ, 490, 577
Elbaz, D., Daddi, E., le Borgne, D., et al., 2007, A&A, 468, 33
Finn, R.A., Zaritsky, D., McCarthy, D.W., Poggianti, B.M., Rudnick, G., Halliday, C., Milvang-Jensen, B., Pello, R., Simard, L., 2005, ApJ, 630, 206
Fritz, J., et al., 2007, A&A, 470, 137
Gladders, M.D., et al., 2007, ApJ, 655, 128
Gomez, P.L., Nichol, R.C., Miller, C.J., et al., 2003, ApJ, 584, 210
Gonzalez, R.E., Padilla, N.D., 2009, MNRAS, 397, 1498
Gray, M.E., Wolf, C., Meisenheimer, K., Taylor, A., Dye, S., Borch, A., Kleinheinrich, M., 2004, MNRAS, 347, L73
Halliday, C. et al., 2004, A&A, 427, 397
Hashimoto, Y., Oemler, A., Lin, H., Tucker, D.L., 1998, ApJ, 499, 589
Hogg, D.W., et al., 2004, ApJ, 601, L29
Kauffmann, G., White, S.D.M., Heckman, T.M., Menard, B., Brinchmann, J., Charlot, S., Tremonti, C., Brinkmann, J., 2004, MNRAS, 353, 713
Kovac, K., et al., 2009, ApJ in press (arXiv:0903.3409)
Lacey, C, Cole, S., 1993, MNRAS, 262, 627
Lewis, I., Balogh, M., De Propris, R. et al., 2002, MNRAS, 334, 673
Lin, Y.-T., Mohr, J.J., Gonzalez, A.H., Stanford, A., 2006, ApJL, 650, L99
Milvang-Jensen, B., et al., 2008, A&A, 482, 419
Peebles, P.J.E., 1993, Principles of physical cosmology, Princeton University Press, Princeton
Poggianti, B.M., et al., 2006, ApJ, 642, 188
Poggianti, B.M. et al., 2008, ApJ, 684, 888
Poggianti, B.M. et al., 2009, ApJ, 693, 112
Popesso, P, Biviano, A., Bohringer, H., Romaniello, M., Voges, W., 2005, A&A, 433, 431
Postman, M., Geller, M.J., 1984, ApJ, 281, 95
Postman, M. et al., 2005, ApJ, 623, 721
Rozo, E., et al. 2009, ApJ, 699, 768
Springel, V., White, S.D.M., Jenkins, A., et al. 2005, Nature, 435, 629
Tasca, L.A.M., et al., 2009, A&A, 503, 379
van Dokkum, P.G., Franx, M., 2001, ApJ, 553, 90
White, S.D. et al., 2005, A&A, 444, 365
Wolf, C. et al., 2009, MNRAS, 393, 1302

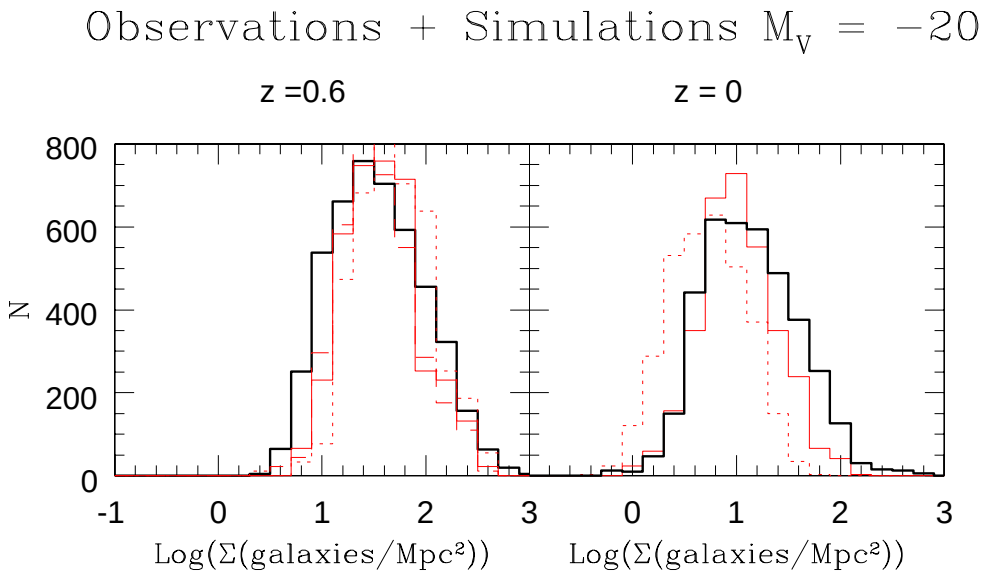

Figure 1. Observed projected local density (galaxies per Mpc^2) distributions (thin histograms, in red) of spectroscopic members within the R_{200} of EDisCS clusters at $z \sim 0.6$ (left panel) and in Sloan clusters at $z = 0.04 - 0.1$ (right panel). They are compared, (thick histograms, in black), with the sim-observed distributions within the projected R_{200} in Millennium Simulation haloes of masses M$> 10^{14}$ at $z = 0.6$ and $z = 0$. A fixed magnitude limit $M_V = -20$ is adopted in both cases. In the case of observations, different density estimates are shown, as described in detail in Poggianti et al. (2008): for EDisCS (left panel), using a statistical background subtraction (short dashed histogram), using photo-z integrated probabilities for membership (thin solid histogram) and the best photo-z estimate (long dashed histogram); for Sloan (right panel), using a statistical background subtraction (thin solid histogram) or using only the spectroscopic catalog (dashed histogram). The latter suffers from spectroscopic incompleteness in SDSS clusters.

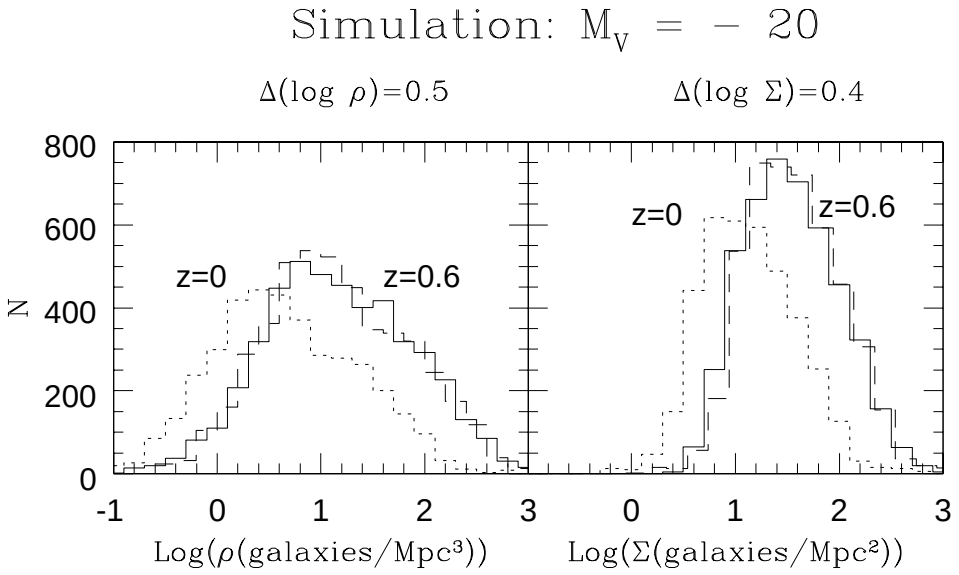

Figure 2. Physical density (left, galaxies per Mpc^3) and sim-observed projected local density (right, galaxies per Mpc^2) distributions of galaxies within the projected R_{200} in Millennium Simulation haloes of masses M$> 10^{14}$ at $z = 0.6$ (solid histograms) and $z = 0$ (dotted histograms). A fixed magnitude limit $M_V = -20$ is adopted at both redshifts. The right panel was compared with the observed projected local density distributions in Fig. 1. The long dashed histogram is the $z = 0$ distribution shifted by 0.5dex (left panel) and 0.4dex (right panel), normalized to the same number of galaxies of the corresponding $z = 0.6$ distribution. The dashed histogram in the right panel has actually been shifted by 0.44dex instead of 0.4 to prevent the histograms from completely overlapping.

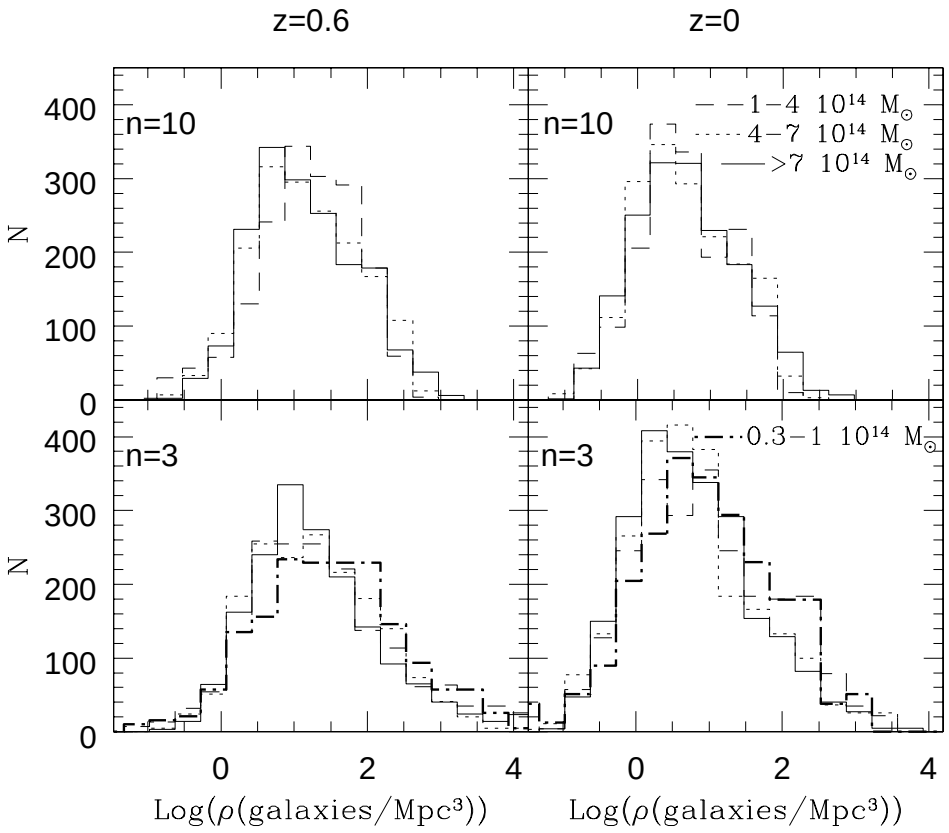

Figure 3. Physical density distribution (galaxies per Mpc^3) of galaxies in Millennium Simulation haloes at $z = 0.6$ (left panels) and $z = 0$ (right panels) for different DM halo mass ranges. Top and bottom panels: density computed using the 10 and 3 closest neighbours, respectively. Halo mass ranges: $> 7\times10^{14}\,M_\odot$ (solid histogram), $4-7\times10^{14}\,M_\odot$ (dotted histogram), $1-4\times10^{14}\,M_\odot$ (dashed histogram), $0.3-1\times10^{14}\,M_\odot$ (heavy dot-dashed histogram, only in bottom panels).

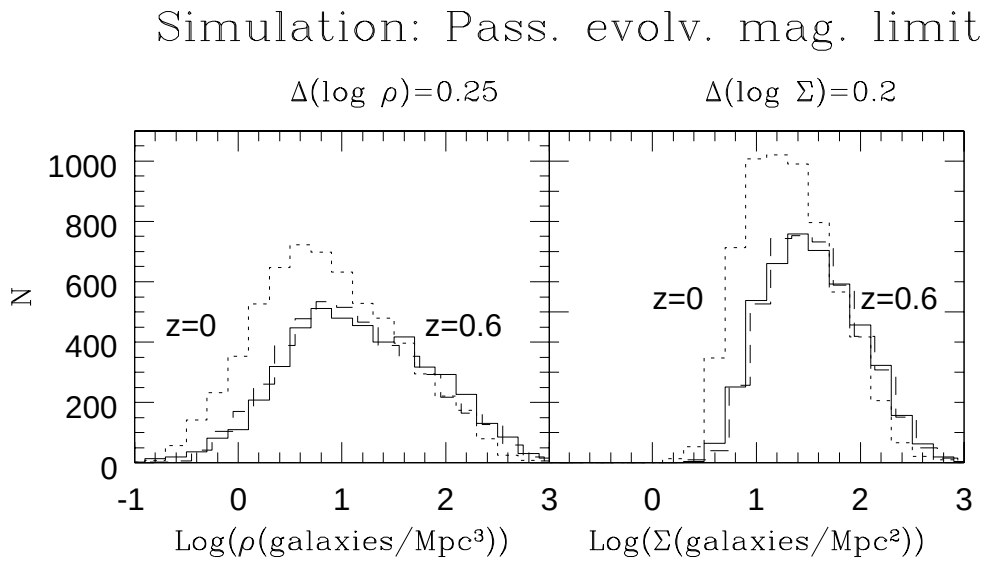

Figure 4. As Fig. 2 but using a passively evolving galaxy magnitude limit: $M_V = -20$ at $z = 0.6$ and $M_V = -19.4$ at $z = 0$. Physical density (left, galaxies per Mpc^3) and sim-observed projected local density (right, galaxies per Mpc^2) distributions of galaxies within the projected R_{200} in Millennium Simulation haloes of masses M$> 10^{14}$ at $z = 0.6$ (filled histograms) and $z = 0$ (dotted histograms). The long dashed histogram is the $z = 0$ distribution shifted by 0.25dex (left panel) or 0.2dex (right panel) normalized to the same number of galaxies as the corresponding $z = 0.6$ distribution. The dashed histogram in the right panel has actually been shifted by 0.24dex instead of 0.2 to prevent the histograms from completely overlapping.

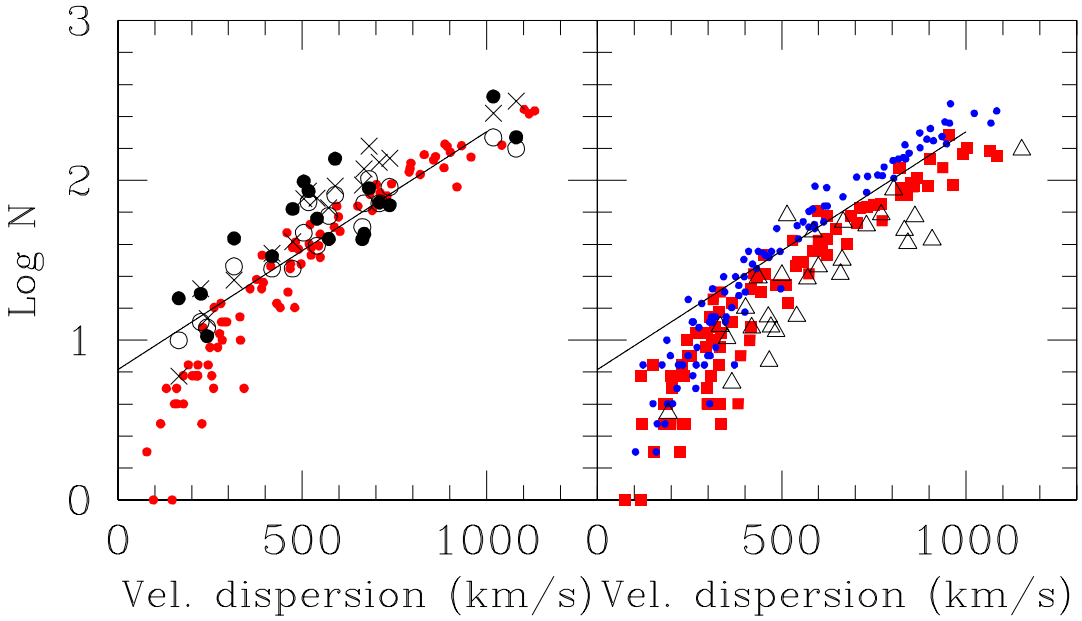

Figure 5. Number of members within R_{200} versus cluster velocity dispersion. **Left: high-z ($z \sim 0.6$).** EDisCS datapoints are black circles (computed using the statistical subtraction), empty circles (computed from photo-z membership) and crosses (computed as the number of spectroscopic members corrected for incompleteness), see text for details. Theoretical (MS) sim-observed values at $z = 0.6$ are represented as small red circles. The solid line is the best linear fit to the theoretical values at $\sigma > 400\,\mathrm{km\,s^{-1}}$. In all cases only galaxies with $M_V \leqslant -20.0$ are included. **Right: low-z ($z \sim 0.07$).** Sloan datapoints at $z = 0.04 - 0.1$ for $M_V \leqslant -20.0$, computed as the number of spectroscopic members corrected for incompleteness, are empty triangles. Theoretical (MS) sim-observed values at $z = 0.0$ for $M_V \leqslant -20.0$ are represented as red squares. The solid line is the best fit to the $z = 0.6$ $M_V \leqslant -20.0$ theoretical values, repeated from the left panel. Blue small points are theoretical values at $z = 0$ adopting a passively evolving galaxy magnitude limit ($M_V \leqslant -19.4$).

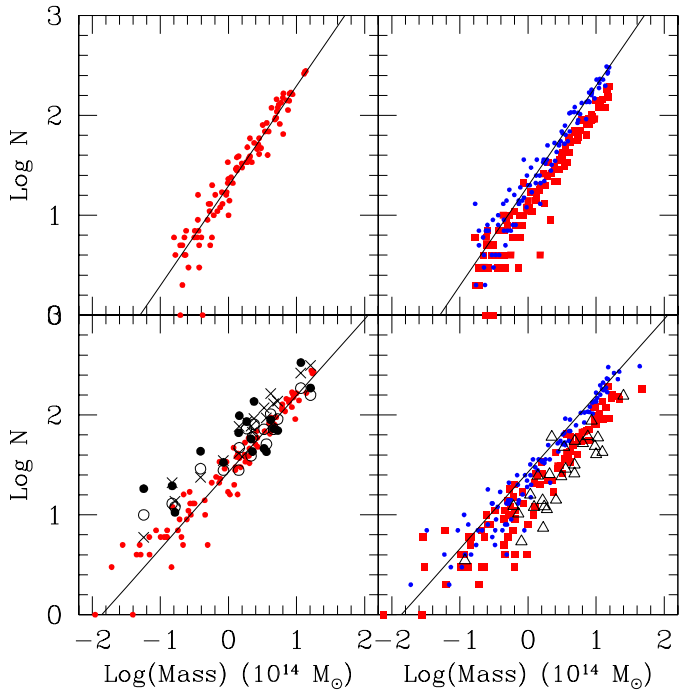

Figure 6. Bottom left and right Number of members within R_{200} versus cluster mass. The cluster mass is computed from the observed or sim-observed velocity dispersion. **Left: high-z** ($z \sim 0.6$). EDisCS datapoints are black circles (computed using the statistical subtraction), empty circles (computed from photo-z membership) and crosses (computed as the number of spectroscopic members corrected for incompleteness). Theoretical (MS) sim-observed values at $z = 0.6$ are represented as small red circles. The solid line is the best linear fit to the theoretical values at $\sigma > 400\,\mathrm{km\,s^{-1}}$, $LogN = (0.77 \pm 0.03) \times LogM + (1.43 \pm 0.02)$. In all cases only galaxies with $M_V \leqslant -20.0$ are included. **Right: low-z** ($z \sim 0.07$). Sloan datapoints at $z = 0.04 - 0.1$ for $M_V \leqslant -20.0$, computed as the number of spectroscopic members corrected for incompleteness, are empty triangles. Theoretical (MS) sim-observed values at $z = 0.0$ for $M_V \leqslant -20.0$ are represented as red squares. The solid line is the best fit to the $z = 0.6$ $M_V \leqslant -20.0$ theoretical values, repeated from the left panel. Blue small points are theoretical values at $z = 0$ adopting a passively evolving galaxy magnitude limit ($M_V \leqslant -19.4$.) **Top left and right** Only simulations are shown, with same symbols as in the bottom panels. The cluster mass plotted is now the dark matter halo mass. The relation steepens, and the slope is now 1: $LogN = (1.00 \pm 0.04) \times LogM + (1.29 \pm 0.02)$.

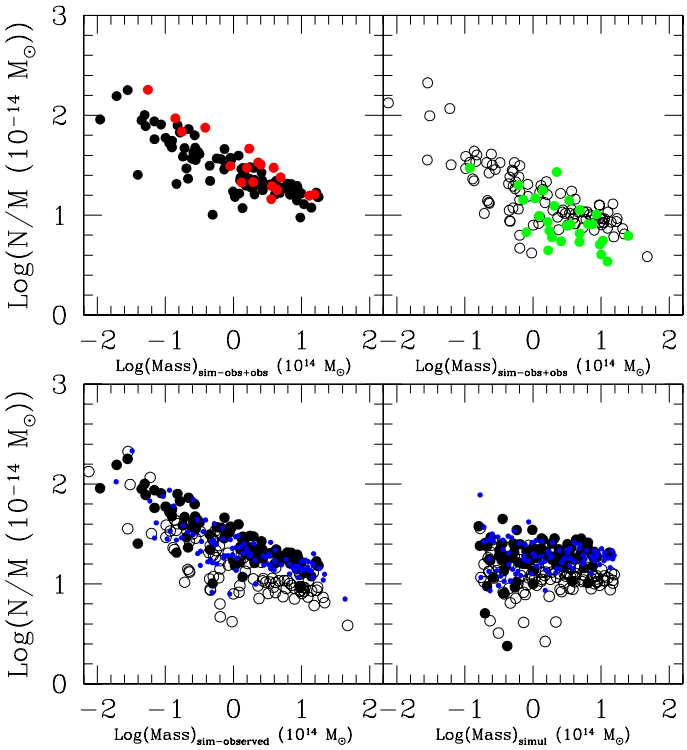

Figure 7. Number of galaxies per unit of cluster mass versus cluster mass. Filled black circles are from simulations at $z = 0.6$ and empty circles are from simulations at $z = 0$, both for a galaxy magnitude limit $M_V = -20$. Blue small dots are the $z = 0$ simulations for $M_V = -19.4$. Observed points for $M_V = -20$ are red (EDisCS) and green (SDSS) points in the top panels. **Bottom left.** Masses, both on the x and y axes, are derived from the sim-observed velocity dispersion. The number of galaxies is the sim-observed number of members. **Bottom right.** Masses, both on the x and y axes, are "true" simulated masses of dark matter haloes. The number of galaxies is the sim-observed number of members. $Log(N/M(10^{-14}M_\odot)) = (1.29 \pm 0.097)$ for haloes with $M > 10^{14}M_\odot$, and $Log(N/M(10^{-14}M_\odot)) = (1.26 \pm 0.217)$ for $M < 10^{14}M_\odot$, computed using together the high-z and the low-z numbers corrected for passive evolution. Results remain unchanged if we use the "real" simulated number of members. **Top left.** The sim-observed results at $z = 0.6$ (filled circles, repeated from the bottom left panel) are compared with the EDisCS observed points (number of spectroscopic members corrected for incompleteness, red circles). Both are for $M_V = -20$. **Top right.** The sim-observed results at $z = 0$ (empty circles, repeated from the bottom left panel) are compared with the Sloan observed points (number of spectroscopic members corrected for incompleteness, green circles). Both are for $M_V = -20$.

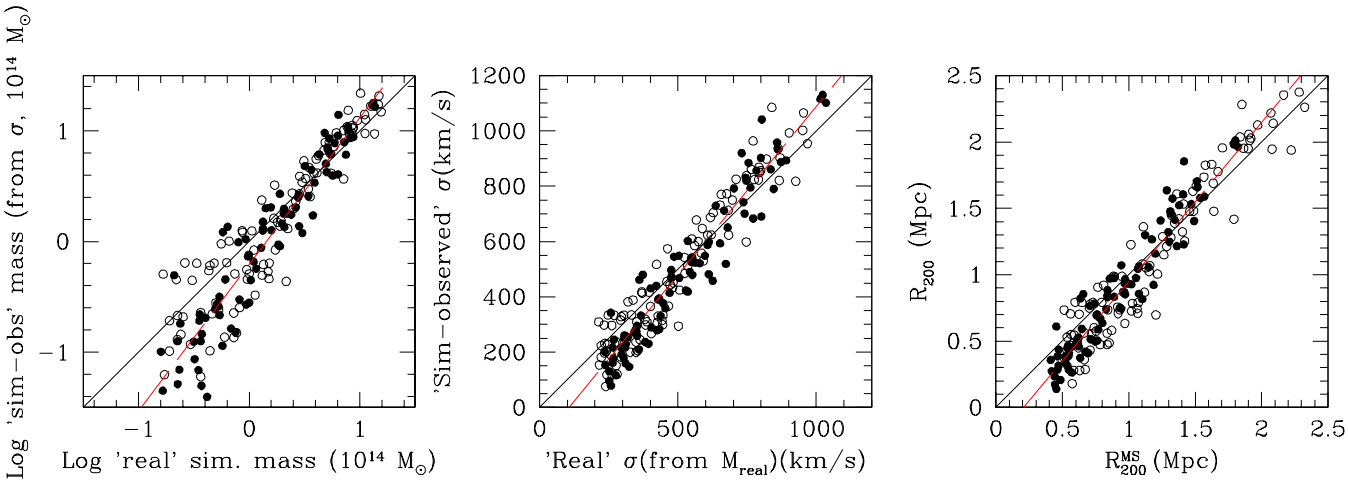

Figure 8. Filled circles are simulation results at $z = 0.6$, and empty circles are at $z = 0$. **Left** The "true" masses of Millennium Simulation haloes are compared with the sim-observed masses of the same haloes computed from the velocity dispersion as it would be observed. The red dashed line is the least square fit $log(M_{sim-obs}) = (1.325 \pm 0.04) \times log(M_{simul}) - (0.21 \pm 0.02)$. The solid line is the 1:1 relation. **Center** The sim-observed velocity dispersion versus the velocity dispersion derived from the "true" halo mass using the M-σ relation given in §5.1. The red dashed line is the least square fit $\sigma_{sim-obs} = (1.22 \pm 0.03) \times \sigma_{simul} - (129 \pm 16)$. The solid line is the 1:1 relation. **Right** The sim-observed R_{200} measured from the simu-observed velocity dispersion using eqn. (1) versus the halo theoretical R_{200}^{MS} radius. The red dashed line is the least square fit $R_{200} = (1.20 \pm 0.03) \times R_{200}^{MS} - (0.25 \pm 0.03)$. The solid line is the 1:1 relation.